

Observing symmetry-broken optimal paths of stationary Kardar-Parisi-Zhang interface via a large-deviation sampling of directed polymers in random media

Alexander K. Hartmann,^{1,*} Baruch Meerson,^{2,†} and Pavel Sasorov^{3,4,‡}

¹*Institut für Physik, Universität Oldenburg - 26111 Oldenburg, Germany*

²*Racah Institute of Physics, Hebrew University of Jerusalem, Jerusalem 91904, Israel*

³*Institute of Physics CAS – ELI Beamlines, 182 21 Prague, Czech Republic*

⁴*Keldysh Institute of Applied Mathematics, Moscow 125047, Russia*

Consider the short-time probability distribution $\mathcal{P}(H, t)$ of the one-point interface height difference $h(x=0, \tau=t) - h(x=0, \tau=0) = H$ of the stationary interface $h(x, \tau)$ described by the Kardar-Parisi-Zhang equation. It was previously shown that the optimal path – the most probable history of the interface $h(x, \tau)$ which dominates the higher tail of $\mathcal{P}(H, t)$ – is described by any of *two* ramp-like structures of $h(x, \tau)$ traveling either to the left, or to the right. These two solutions emerge, at a critical value of H , via a spontaneous breaking of the mirror symmetry $x \leftrightarrow -x$ of the optimal path, and this symmetry breaking is responsible for a second-order dynamical phase transition in the system. Here we employ a large-deviation Monte Carlo sampling algorithm in conjunction with the mapping between the KPZ interface and the directed polymer in a random potential at high temperature. This allows us to observe the optimal paths, which determine each of the two tails of $\mathcal{P}(H, t)$, down to probability densities as small as 10^{-500} . The observed mirror-symmetry-broken traveling optimal paths for the higher tail, and mirror-symmetric paths for the lower tail, are in good quantitative agreement with analytical predictions.

I. INTRODUCTION

Large deviations in stochastic macroscopic systems out of equilibrium continue to attract much interest from the statistical mechanics community. Of special interest are situations where the large-deviation functions exhibit singularities. These singularities can be classified as dynamical phase transitions (DPTs), see Refs. [1–5] for reviews. It was shown recently [6, 7] that the list of system exhibiting DPTs includes the Kardar-Parisi-Zhang (KPZ) equation [8] in 1+1 dimension:

$$\partial_\tau h = \nu \partial_x^2 h + (\lambda/2) (\partial_x h)^2 + \sqrt{D} \xi(x, \tau). \quad (1)$$

This celebrated equation describes the stochastic dynamics of the height $h(x, \tau)$ at point x and at time τ of an interface driven by a delta-correlated Gaussian noise $\sqrt{D} \xi(x, \tau)$ with zero mean:

$$\begin{aligned} \langle \xi(x, \tau) \rangle &= 0, \\ \langle \xi(x_1, \tau_1) \xi(x_2, \tau_2) \rangle &= \delta(x_1 - x_2) \delta(\tau_1 - \tau_2). \end{aligned} \quad (2)$$

In Eq. (1) $\nu > 0$ is the diffusion constant, and the non-linearity coefficient λ can be set to be positive (or negative) without loss of generality.

In Refs. [6, 7], and in the present work, the fluctuating quantity of interest is the interface height difference $h(x=0, \tau=t) - h(x=0, \tau=0) = H$ at a specified point $x=0$ at time t [9]. The complete statistics of the height difference of the KPZ interface has been in the focus of multiple recent studies, see Refs. [10–12] for reviews.

We will be interested in the short-time regime, when the current time t is much smaller than the characteristic nonlinear time of the KPZ equation $t_{\text{NL}} = \nu^5 / (D^2 \lambda^4)$ [13]. At short times typical fluctuations of the KPZ interface, which corresponds to the body of the probability distribution $\mathcal{P}(H, t)$, are still Gaussian. However, the KPZ nonlinearity is already fully manifest in the tails of $\mathcal{P}(H, t)$. The distribution $\mathcal{P}(H, t)$ depends on the initial condition $h(x, \tau=0)$. The DPT [6, 7] occurs, in the short-time regime, for the *stationary* initial condition, where it is assumed that the interface has evolved for a long time prior to $\tau=0$. For the stationary interface the initial configuration $h(x, \tau=0)$ is sampled from a statistical ensemble of random realizations of a two-sided Brownian motion:

$$h(x, \tau=0) = \sqrt{\frac{D}{\nu}} B(x), \quad (3)$$

where $B(x)$ is the two-sided Wiener process with diffusion constant 1 [14]. At short times, the probability distribution $\mathcal{P}(H, t)$ scales, up to a pre-exponential factor, as [6, 15]

$$-\ln \mathcal{P}(H, t) \simeq \frac{\nu^{5/2}}{D \lambda^2 \sqrt{t}} s \left(\frac{|\lambda| H}{\nu} \right). \quad (4)$$

The function

$$S(H) = -\lim_{t \rightarrow 0} \sqrt{t} \ln \mathcal{P}(H, t) = \frac{\nu^{5/2}}{D \lambda^2} s \left(\frac{|\lambda| H}{\nu} \right) \quad (5)$$

is the short-time large deviation function. Remarkably, $S(H)$ exhibits a second-order DPT (that is a jump in the second derivative $d^2 S / dH^2$) at a critical value of H such that $\lambda H_c / \nu = 3.7063 \dots$. This DPT originates from a spontaneous breaking of mirror symmetry of the optimal

* a.hartmann@uni-oldenburg.de

† meerson@mail.huji.ac.il

‡ pavel.sasorov@gmail.com

path which we will discuss shortly. A rather complete analogy of this DPT with the classical mean-field second-order transition in equilibrium was established in Ref. [7], where a proper phase order parameter was identified, and an effective Landau theory was developed.

Ref. [6] also determined the large- $|H|$ asymptotics of $S(H)$

$$S(H) \simeq \begin{cases} \frac{4\sqrt{2}\nu}{3D|\lambda|^{1/2}} |H|^{3/2}, & \lambda H \rightarrow +\infty, \\ \frac{4\sqrt{2|\lambda|}}{15\pi D} |H|^{5/2}, & \lambda H \rightarrow -\infty, \end{cases} \quad (6)$$

which correspond to the (stretched-exponential) higher and lower tails of the distribution $\mathcal{P}(H, t)$. The high tail (6) also holds at long times [16, 17], and the same is conjectured to be true, for sufficiently large $|H|$, for the low tail (7). In this paper we report our observations of the *optimal paths* of the KPZ interface, which determine the distribution tails (6) and (7), in numerical simulations.

The results of Refs. [6, 7] were obtained by the optimal fluctuation method (OFM) (see also Ref. [18]). The OFM – by now a standard asymptotic tool of theoretical physics – relies on a saddle-point evaluation of the path integral of the KPZ equation (1), conditioned on the specified large height H . This procedure brings about a classical field theory, formulated as a conditional variational problem. The solution of this problem, obeying the proper initial and boundary conditions, is called the optimal path of the conditioned process. It represents a time-dependent deterministic field which describes the most probable time history of the system, dominating the contribution of different paths to the statistics of interest. The OFM has been extensively used for studying the single-point height statistics of the KPZ equation in different settings and dimensions and for different initial conditions [19–31].

Let $\lambda > 0$. Crucially, at $H > H_c$ the OFM predicts the existence of *two* optimal paths of the interface [6, 7]. The two optimal solutions appear at the critical point $H = H_c$ via a spontaneous breaking of the mirror symmetry – the spatial reflection symmetry $x \leftrightarrow -x$, leading to the second-order DPT. Each of the two optimal solutions is a mirror-symmetric “twin” of the other with respect to $x \leftrightarrow -x$. At large positive H each of the two solutions has the form of a ramp-like traveling structure of $h(x, \tau)$ or, equivalently, a shock-antishock pair of the interface slope $V(x, \tau) = \partial_x h(x, \tau)$. For $-\infty < H < H_c$, that is below the transition, the optimal path is unique and mirror symmetric [6, 7, 23].

Optimal paths give a valuable insight into the physics of large deviations, and this insight is inaccessible by other methods. However, a direct observation of optimal paths in standard numerical simulations (and of course in experiments) is often difficult due to the very low probability of the large deviations in question [32]. Fortunately, this difficulty can be overcome by using large-deviation algorithms, *e.g.* based on importance sampling

approaches, as was recently shown for the KPZ equation in Refs. [33–35]. In these works a standard mapping from the KPZ equation to the (discrete) directed polymer in a random potential at high temperature was employed, and Monte-Carlo simulations with an importance sampling algorithm were performed. As a result, the tails of the KPZ interface height distribution were measured, for different initial conditions and at different times, down to probabilities as small as 10^{-1000} [33, 35]. In particular, Ref. [35] measured the tails of $\mathcal{P}(H, t)$ at short times for the stationary interface and verified the asymptotics (6) and (7). In Ref. [34] the interface configurations at $\tau = t/2$, corresponding to the height distribution tails at $\tau = t$, were observed for the *sharp-wedge* initial condition. The observed configurations turned out to be in good agreement with those predicted from the OFM [23].

Here we employ the same simulation strategy as in Refs. [33–35] to observe the optimal paths of the stationary KPZ interface which correspond to the distribution tails (6) and (7). We clearly observe two mirror-symmetry-broken traveling optimal paths for the higher tail, and a single mirror-symmetric path for the lower tail. The optimal paths turn out to be in good quantitative agreement with the predictions from the OFM [6, 7]. In Sec. II we present, and elaborate on, theoretical predictions of Refs. [6, 7] for the optimal paths. In Sec. III we present our simulation strategy and compare the simulation results with theory. In Sec. IV we briefly summarize our results.

II. OPTIMAL PATHS: THEORETICAL PREDICTIONS

Here we present and slightly extend the theoretical predictions of Refs. [6, 7]. To be in line with the notation of Refs. [6, 7], we will temporarily switch to the convention $\lambda < 0$. The final results of this section will be presented in a fully dimensional form with an arbitrary sign of λ . Introduce rescaled variables $\tau/t \rightarrow \tau$, $x\sqrt{\nu t} \rightarrow x$ and $|\lambda|h/\nu \rightarrow h$. Then Eq. (1) becomes dimensionless:

$$\partial_\tau h = \partial_x^2 h - \frac{1}{2} (\partial_x h)^2 + \sqrt{\epsilon} \xi(x, \tau), \quad (8)$$

where $\epsilon = D\lambda^2\sqrt{t}/\nu^{5/2} = (t/t_{\text{NL}})^{1/2}$ is the rescaled noise magnitude. We choose the reference frame of the interface position so that

$$h(x=0, \tau=0) = 0 \quad (9)$$

and condition the rescaled stochastic process $h(x, \tau)$ on the equality

$$h(x=0, \tau=1) = H, \quad (10)$$

where H is rescaled by $\nu/|\lambda|$. The OFM formally demands that $\epsilon \rightarrow 0$, but it actually holds, sufficiently far in the height distribution tails, for any ϵ . The saddle-point procedure brings about a minimization problem for an

effective action functional $s[h(x, \tau)]$. For the stationary interface this functional includes two terms [6]:

$$s[h(x, \tau)] = s_{\text{dyn}}[h(x, \tau)] + s_{\text{in}}[h(x, 0)], \quad (11)$$

where

$$s_{\text{dyn}}[h(x, \tau)] = \frac{1}{2} \int_0^1 d\tau \int_{-\infty}^{\infty} dx \left[\partial_\tau h - \partial_x^2 h + \frac{1}{2} (\partial_x h)^2 \right]^2 \quad (12)$$

is the dynamical contribution, whereas

$$s_{\text{in}}[h(x, 0)] = \int_{-\infty}^{\infty} dx (\partial_x h)^2 \Big|_{\tau=0} \quad (13)$$

is the “cost” of the initial height profile [6]. The ensuing Euler-Lagrange equation can be recast in the Hamiltonian form

$$\partial_\tau h = \partial_x^2 h - \frac{1}{2} (\partial_x h)^2 + \rho, \quad (14)$$

$$\partial_\tau \rho = -\partial_x^2 \rho - \partial_x (\rho \partial_x h), \quad (15)$$

where $\rho(x, \tau)$, the optimal realization of the (rescaled) noise $\xi(x, \tau)$, plays the role of the “momentum density” field, which is canonically conjugate to the “coordinate density”, which is the optimal path $h(x, \tau)$ itself.

The minimization over $h(x, \tau = 0)$ yields an initial condition in the form of a relation between *a priori* unknown $h(x, 0)$ and $\rho(x, 0)$ [6]:

$$\rho(x, \tau = 0) + 2\partial_x^2 h(x, \tau = 0) = \Lambda \delta(x). \quad (16)$$

This condition is specific to the stationary interface. The one-point condition (10) leads to the singular condition

$$\rho(x, \tau = 1) = \Lambda \delta(x), \quad (17)$$

where Λ , which plays the role of a Lagrangian multiplier, is to be ultimately expressed through H .

It was discovered in Ref. [7] that the entire OFM formulation (14)-(17) is invariant under the transformation

$$h(x, \tau) \rightarrow H - h(-x, 1 - \tau), \quad (18)$$

$$\rho(x, \tau) \rightarrow \rho(-x, 1 - \tau) + 2\partial_x^2 h(-x, 1 - \tau). \quad (19)$$

In what follows we will exploit the symmetry

$$h(x, \tau) = H - h(-x, 1 - \tau) \quad (20)$$

which is respected by both the mirror-symmetric optimal paths, and the mirror-symmetry broken paths [7]. In the former case, where $h(-x, \tau) = h(x, \tau)$, Eq. (20) simplifies to

$$h(x, \tau) = H - h(x, 1 - \tau). \quad (21)$$

Once the optimal path, including the optimal initial height profile, is determined, one can evaluate the rescaled total action (11), and obtain the function $s = s(H)$ which enters Eqs. (4) and (5).

In Refs. [6] and [7] asymptotic solutions of the OFM problem (14)-(17) were obtained in the two limits, corresponding to the high and low tails of \mathcal{P} and described by Eqs. (6) and (7), respectively. In Sections II A and II B we present the corresponding optimal solutions for $h(x, t)$, to be compared with our simulations in Sec. III C.

A. Optimal path for the high tail $\lambda H > 0$

Here we use the dimensional variables. At supercritical values of H there are two mirror-symmetry broken optimal paths [6]. In the $\lambda H \rightarrow +\infty$ tail, each of them represents a simple ramp-like structure for $h(x, \tau)$ [or, equivalently, a shock-antishock pair of the interface slope $V(x, \tau) = \partial_x h(x, \tau)$], traveling to the left or to the right. In terms of $h(x, \tau)$ the left-traveling ramp has the form [6]:

$$h(x, \tau) \simeq \begin{cases} 1, & x \geq \ell(1 - t), \\ \frac{x}{\ell} + t, & -\ell t \leq x \leq \ell(1 - t), \\ 0, & x \leq -\ell t. \end{cases} \quad (22)$$

$$\frac{h(x, \tau)}{H} \simeq \begin{cases} 1, & x \geq \ell(1 - t), \\ \frac{x}{\ell} + t, & -\ell t \leq x \leq \ell(1 - t), \\ 0, & x \leq -\ell t. \end{cases} \quad (23)$$

where $t = \tau/t$ and

$$\ell = \ell(H, t) = \left(\frac{|\lambda H| t}{2} \right)^{1/2}. \quad (25)$$

By virtue of the symmetry (20), the right-traveling ramp solution can be obtained from Eqs. (22)-(24) by replacing x by $-x$ and τ by $t - \tau$ (that is, t by $1 - t$). Snapshots of the right- and left-traveling solutions for $h(x, \tau)$ are depicted in Fig. 1.

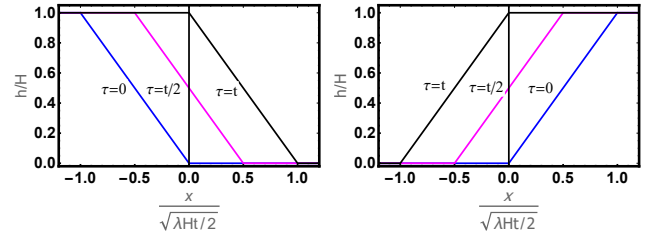


FIG. 1. Two mirror-symmetry broken optimal paths corresponding to the high tail, $\lambda H > 0$, of the height distribution $\mathcal{P}(H, t)$, see Eq. (6). Shown is the leading-order prediction of Ref. [6] for $h(x, \tau)$ as described by Eqs. (22)-(24) for the ramp traveling to the left (the right panel), and its mirror reflection with respect to $x = 0$ for the ramp traveling to the right (the left panel).

B. Optimal path for the low tail $\lambda H < 0$

In the leading order in $\lambda H \rightarrow -\infty$ the solution is very different [6, 7, 22, 23]. In particular, it does not depend on the diffusion constant ν , ultimately leading to the ν -independent asymptotic (7) of $S(H)$. In the “pressure-dominated” region the solution describes an ideal hydrodynamic flow of an effective gas with density $\rho(x, \tau)$, velocity $V(x, \tau) = \partial_x h(x, \tau)$ and a negative pressure $-(1/2)\rho^2(x, \tau)$. There are also a region of a zero-pressure hydrodynamic flow (also called the Hopf flow) [7] and a trivial “static region” where $h(x, \tau) = H/2 = \text{const}$.

The results of Refs. [6, 7, 22, 23] were presented in terms of $V(x, \tau)$ rather than $h(x, \tau)$, but the latter can

be determined from the former by integration over x . After some algebra we obtained, in the three regions,

$$\frac{h(x, \tau)}{H} \simeq \begin{cases} \mathfrak{h}_g\left(\frac{\pi x}{2\ell}, \mathfrak{t}\right) + \frac{1}{2}, & \frac{\pi|x|}{2} < \frac{\ell}{1+w(\mathfrak{t})^2}, \end{cases} \quad (26)$$

$$\frac{h(x, \tau)}{H} \simeq \begin{cases} \mathfrak{h}_v\left(\frac{\pi|x|}{2\ell}, \mathfrak{t}\right) + \frac{1}{2}, & \frac{\ell}{1+w(\mathfrak{t})^2} < \frac{\pi|x|}{2} < \ell, \end{cases} \quad (27)$$

$$\frac{h(x, \tau)}{H} \simeq \begin{cases} \frac{1}{2}, & \frac{\pi|x|}{2} > \ell. \end{cases} \quad (28)$$

where ℓ is defined in Eq. (25), and we have introduced three functions: w , \mathfrak{h}_g , and \mathfrak{h}_v . The function $w(\mathfrak{t})$ is the inverse of the function

$$\mathfrak{t} = \frac{1}{2} + \frac{w}{\pi(1+w^2)} + \frac{1}{\pi} \arctan w, \quad (29)$$

the function $\mathfrak{h}_g(\chi, \mathfrak{t})$ is defined explicitly:

$$\mathfrak{h}_g(\chi, \mathfrak{t}) = \frac{1}{\pi} \arctan w(\mathfrak{t}) - \frac{1}{\pi} w(\mathfrak{t}) [1 + w^2(\mathfrak{t})] \chi^2, \quad (30)$$

and the function $\mathfrak{h}_v(\chi, \mathfrak{t})$ is defined in a parametric form:

$$\mathfrak{h}_v(z, \mathfrak{t}) = u^2 \left(\mathfrak{t} - \frac{1}{2} \right) + \frac{1}{\pi} [u + (u^2 - 1) \arctan u], \quad (31)$$

$$z = \pi u \left(\mathfrak{t} - \frac{1}{2} \right) + 1 + u \arctan u, \quad (32)$$

where the domain of u in Eqs. (31)-(32) are defined by the double inequality

$$-w(\mathfrak{t}) \left(\mathfrak{t} - \frac{1}{2} \right) < u \left(\mathfrak{t} - \frac{1}{2} \right) < 0. \quad (33)$$

Overall, the optimal h -profile (26)-(28) as a function of x at different times $0 \leq \tau \leq t$ is depicted in Fig. 2. Notice, that the optimal initial height profile has a plateau at $h = H/2$ at large $|x|$. This property holds for all subcritical values of H : $-\infty < \lambda H < |\lambda| H_c$, where the mirror symmetry of the optimal path is preserved.

III. SIMULATIONS

A. Directed polymer mapping

Let us recall the lattice version of the mapping between the KPZ height $h(x, t)$ and the free energy of a directed polymer in a two-dimensional random potential at high temperature T [36]. It is convenient for our purposes to consider a right-triangular domain, defined on a half square lattice with side length L as shown in Fig. 3. The lattice is indexed by points (x, τ) with $\tau = 0, 1, \dots, t$ ($t = 2L$) playing the role of a time and $x = -x_{\max}, -x_{\max} + 1, \dots, x_{\max} - 1, x_{\max}$ where $x_{\max} = (t - \tau)/2$. We consider all directed polymers which start at a lattice point on the hypotenuse $(x, 0)$ and end at the apex $(0, 2L)$. The random value of the potential V at each lattice point is normally distributed with zero mean and unit variance.

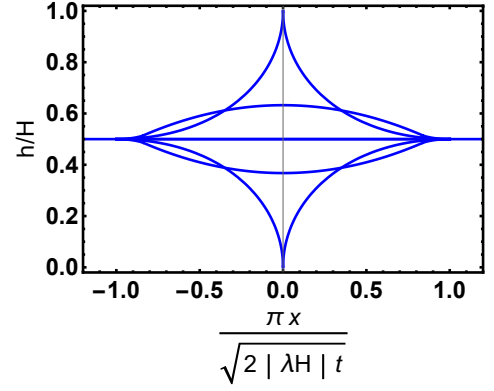


FIG. 2. The mirror-symmetric optimal paths corresponding to the low tail, $\lambda H < 0$, of the height distribution $\mathcal{P}(H, t)$, see Eq. (7). Shown are the leading-order theory prediction for $h(x, \tau)$ vs x as described by Eqs. (26)-(28) at rescaled times $\mathfrak{t} = \tau/t = 0, 0.25, 0.5, 0.75$, and 1 (from bottom to top; the horizontal line displays $t = 0.5$).

The partition function $Z(x, \tau)$ of a given realization of the potential obeys the exact recursive equation [36]

$$Z(x, \tau + 1) = \left[Z\left(x - \frac{1}{2}, \tau\right) + Z\left(x + \frac{1}{2}, \tau\right) \right] e^{-\frac{V(x, \tau+1)}{T}}, \quad (34)$$

where $\langle V(x, \tau) V(x', \tau') \rangle = \delta_{xx'} \delta_{\tau\tau'}$, and $\delta_{xx'}$ and $\delta_{\tau\tau'}$ are Kronecker deltas.

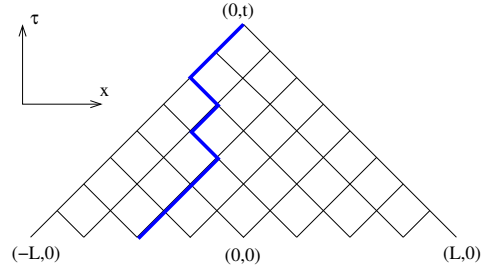


FIG. 3. A lattice realization of the directed polymer (see the text). $t = 2L$.

Let us introduce $Z^*(x, \tau) = 2^{-\tau} Z(x, \tau)$. To obtain the mapping from the discrete Eq. (34) to the continuous KPZ equation (1) we Taylor-expand all the discrete quantities in Eq. (34), including $\exp(-V/T)$. For example,

$$Z^*\left(x - \frac{1}{2}, \tau\right) = Z^*(x, \tau) - \frac{1}{2} \partial_x Z^*(x, \tau) + \frac{1}{8} \partial_x^2 Z^*(x, \tau) + \dots \quad (35)$$

To justify a truncation of this expansion we must demand that Z^* varies slowly on the scale of the lattice constant both in space and in time: $|Z^*(x, \tau + 1) - Z^*(x, \tau)| \ll Z^*(x, \tau)$ and $|Z^*(x + 1, \tau) - Z^*(x, \tau)| \ll Z^*(x, \tau)$. This leads to the necessary conditions $L \gg 1$ and $|H| \ll L$. As we are studying large deviations, we consider $|H| \gg 1$. Finally, the slow variation of the potential V necessitates

the condition $T \gg 1$. Overall, these necessary conditions can be rewritten as a strong double inequality

$$1 \ll |H| \ll L. \quad (36)$$

Under these conditions we can approximate the discrete Eq. (34) by the stochastic heat equation

$$\partial_\tau Z^* = \frac{1}{8} \partial_x^2 Z^* - \frac{\xi}{T} Z^*. \quad (37)$$

The noise term ξ is now continuous and delta-correlated in x and τ , and the mapping to the KPZ equation is given by the Cole-Hopf transformation

$$h(x, \tau) = \ln[Z^*(x, \tau) / \langle Z^*(0, \tau) \rangle], \quad (38)$$

where

$$\lambda = 1/4, \quad \nu = 1/8, \quad D = T^{-2} \quad \text{and} \quad t = 2L. \quad (39)$$

The characteristic nonlinear time of the KPZ equation, $t_{\text{NL}} = \nu^5 / (D^2 \lambda^4) = T^4 / 2^7$. In particular, the height difference is given by

$$H = h(0, 2L) = \ln[Z^*(0, 2L) / \langle Z^*(0, 2L) \rangle]. \quad (40)$$

The Brownian initial condition is specified by

$$Z(x, 0) = e^{-[V(x, 0) + 2R(x)]/T}, \quad (41)$$

where $R(x) = \sum_0^x \eta(x)$ describes a random walk starting at the origin $(0, 0)$ and arriving at the site $(x, 0)$ on the hypotenuse, where $-L \leq x \leq L$. The random walk increments $\eta(x)$ are independent and normally distributed random numbers with zero mean and variance 1.

B. Importance sampling algorithm

All measurable quantities, like the height difference H , depend on the set of calculated partition function values $\{Z(x, \tau)\}$. Furthermore, the partitions function values depend through Eqs. (34) and (41) deterministically on the realization (V, η) of the quenched randomness, with V being the set of $(L+1)(2L+1)$ potential values $\{V(-L, 0), V(-L+1, 0), \dots, V(L-1, 0), V(L, 0), V(-L+\frac{1}{2}, 1), V(-L+\frac{3}{2}, 1), \dots, V(-\frac{1}{2}, 2L-1), V(\frac{1}{2}, 2L-1), V(0, 2L)\}$ and η being the set of $2L+1$ random walk increments $\{\eta(-L), \eta(-L+1), \dots, \eta(L-1), \eta(L)\}$. As we already mentioned, all these random values are independent and normally distributed with zero mean and variance 1.

A straightforward way to sample measurable quantities would be to generate independent realizations (V, η) of the disorder, to calculate the partition function for each realization and obtain the desired quantity. In this way estimates for expectation values can be obtained by averages, possibly conditioned on certain values of a second observable, like H . Estimates for distributions are obtained from histograms.

This procedure, however, would generate *typical* values with respect to all quantities, in particular typical values with respect to H . In the present study we are rather interested in investigating the behavior of the system for very rare values of H . Thus, we have to be able to address the underlying distribution $\mathcal{P}(H)$ over a large part of the support, in particular the low-probability tails.

To achieve this, we use a *biased* distribution [37] of the randomness by modifying the original quenched distribution weight [38], which is a product of independent Gaussians, by an additional exponential Boltzmann factor $e^{-H/\Theta}$, where Θ is an adjustable temperature-like parameter, allowing us to address different regions of values of H . When $\Theta \rightarrow \pm\infty$, we restore the original unbiased distribution. For $\Theta \rightarrow 0^+$, one will focus the sampling on large negative values of H , while for $\Theta \rightarrow 0^-$ the sampling will be in the region of large positive values of H . The fundamental idea of this large-deviation approach is versatile and it has been applied to various problems, e.g., to study large-deviation properties of random graphs [39, 40], of random walks [41, 42] of energy grids [43, 44], of biological sequence alignments [38, 45], of nonequilibrium work distributions [46], and of traffic models [47].

Note that any obtained statistics will initially follow the biased weight, but this can be easily corrected by reweighting with the inverse weight, i.e., $e^{+H/\Theta}$, and proper normalization [38]. This is important if one is interested in actually measuring $\mathcal{P}(H)$. In the present case, we do not need to do this, because we only want to measure some other quantities which are conditioned on certain, e.g., extreme values of H . Thus, we only have to be able to sample with respect to selected values of H , which is achieved by the bias.

In the present case, the biased sampling of the disorder realizations (V, η) cannot be performed directly. Therefore we applied Markov-chain Monte Carlo (MC) simulations [48], where a configuration of the Markov chain at step s is given by a disorder realization $(V, \eta)^{(s)}$. As explained above, the corresponding height depends deterministically on the disorder realizations, i.e. $H^{(s)} = H[(V, \eta)^{(s)}]$. Following the Metropolis-Hastings algorithm, in each step some of the entries of $(V, \eta)^{(s)}$ are redrawn according to the underlying Gaussian distribution, leading to a trial configuration $(V, \eta)'$ which corresponds to a value H' . This value has to be obtained in each MC step by a full calculation of the partition function using Eqs. (34) and (41) and finally evaluating H' with Eq. (40). To obtain a sampling according to the biased distribution, the trial configuration is accepted, i.e. $(V, \eta)^{(s+1)} = (V, \eta)'$, with the usual Metropolis probability $p_{\text{acc}} = \min\{1, e^{-\Delta H/\Theta}\}$ depending on the change $\Delta H = H' - H^{(s)}$. Otherwise the trial configuration is rejected, i.e. $(V, \eta)^{(s+1)} = (V, \eta)^{(s)}$. As usual, one has to make the MC simulations long enough to achieve equilibration and avoid correlated configurations. For more details on the implementation of the large-deviation algorithm for the KPZ model, including the choice of the values for Θ , the combination of the results obtained for

different values of Θ , the use of the parallel tempering approach, and the parallelization using Message Passing Interface, see Refs. [33, 35].

For all simulations the parameters of the directed polymer model were $t = 2L = 128$ and $T = 8$. We performed a parallel tempering simulation for a total of 478 different values of the temperatures Θ on a high-performance computer which required a total of more than 73000 core hours. During the parallel simulation, we monitored equilibration by following the convergence of the statistics of H . The convergence takes different time scales depending on the values of Θ . During the simulation, we have stored about 23000 configurations with values of H ranging in the interval $[-58, 86]$. The configurations are spread with respect to H more or less equally over this interval, but with an emphasis on the extremes of the interval, because more values of the temperature Θ are needed to sample in equilibrium in this range.

C. Theory versus simulations

Here we present the simulation results and compare them with the theoretical predictions for the set of parameters (39). We will start from the case of $H > 0$, where breaking of the mirror symmetry occurs, and then proceed to the case of $H < 0$ where the mirror symmetry is preserved. For the chosen parameters $T = 8$ and $L = 64$ of the directed polymer model, the ratio of $t/t_{\text{NL}} = 4$ is not a small number, but it still corresponds to the short-time limit [13].

1. Large positive H

In the range $10 \leq H \leq 30$, we obtained 935 independent realizations (V, η) , each allowing for an analysis of the trajectories of $h(x, \tau)$ for all values $\tau \in [0, 1]$. (Note that for standard sampling, realizations exhibiting such values of H would occur with their natural probabilities which are 10^{-100} or smaller [35], so we indeed needed to employ large-deviations algorithms to study this range of H .) We clearly observed the mirror symmetry breaking in the form of left- and right-traveling ramps of $h(x, \tau)$. To improve the statistics, we flipped around $x = 0$ the observed $h(x, \tau)$ profiles of the right-travelling ramp realizations and processed them together with the left-travelling-ramps. The resulting Fig. 4 shows the average over all the simulated $h(x, \tau)$ -profiles for $H \simeq 20$ at $\tau/t = 0, 0.35$ and 0.65 . The error bars are small, and the traveling ramp structure is remarkably pronounced. Figure 5 shows, at $\tau = 0.5t$, that the theoretically-predicted asymptotic [6], described by Eqs. (22)-(24), is in good agreement with the simulated ramp profile. The observed discrepancies ($\lesssim 5\%$ in terms of H) can be attributed to effects of finite $1/H$ and H/L , see Eq. (36).

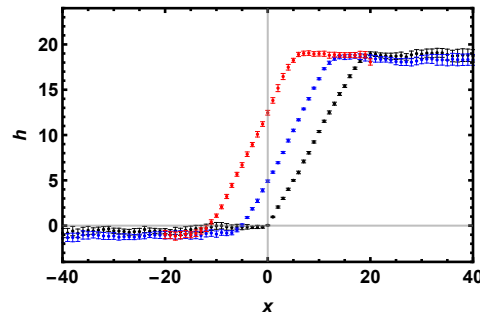


FIG. 4. The average over 9 simulated optimal height profiles $h(x, \tau)$ at rescaled times $\tau/t = 0$ (black), 0.35 (blue), and 0.65 (red) for $H \simeq 20$. The actual values of H are $H \in [19.95, 20.1]$. Eight of these height profiles are actually *right-travelling* ramps flipped around $x = 0$. The error bars show the standard deviation. The simulation parameters are $T = 8$ and $L = 64$.

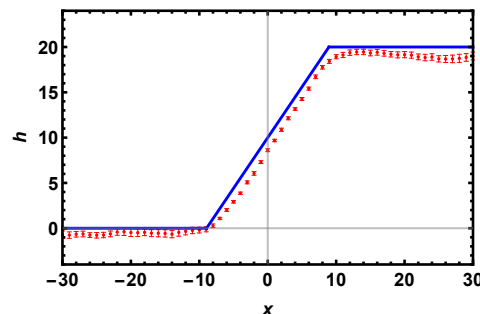


FIG. 5. A comparison, at time $\tau = 0.5t$, of the simulated optimal height profile at $H \simeq 20$ (see Fig. 4) with the asymptotic traveling ramp solution [6], described by Eqs. (22)-(24).

2. Large negative H

Figure 6 shows the average over 60 simulated h -profiles for $H \simeq -20$ (the actual values $H \in [-20.2, -20]$). Realizations exhibiting such values of H appear with natural probabilities about 10^{-450} or smaller [35]. Also shown is the theoretically-predicted asymptotic for $H = -20$, see Eqs. (26)-(28). The mirror symmetry is manifestly preserved here. Again, the discrepancy between the asymptotic theory and simulations is of order of 5% in terms of $|H|$, and it can be attributed to finite $|H|/L$ effects. Indeed, we also simulated the case of $H \simeq -40$ (not shown here) and found that the discrepancy between our theory (which assumes $|H| \ll L$) and the simulations becomes quite large.

IV. SUMMARY AND DISCUSSION

Optimal paths provide an instructive and fascinating characterization of a whole class of large deviations in non-equilibrium stochastic systems. By combining the mapping between the KPZ interface and the di-

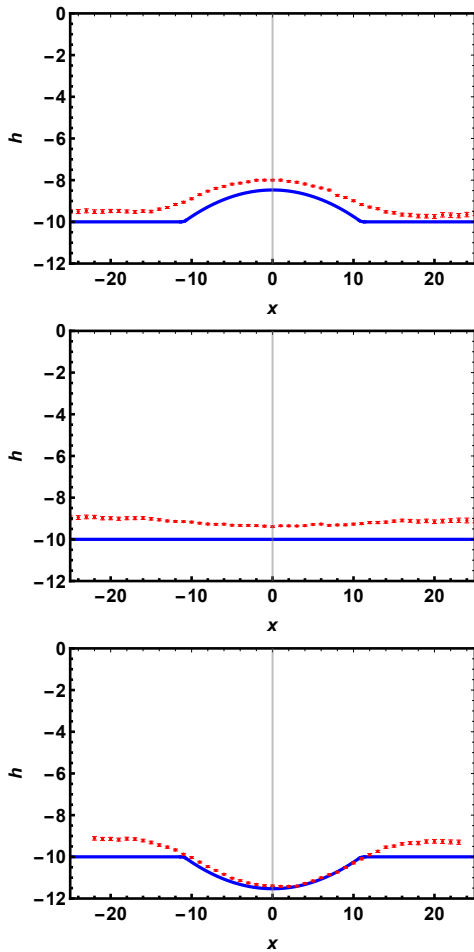


FIG. 6. A comparison of the simulated optimal height profile at $H \simeq -20$ (the red points with error bars) with the asymptotic solution for $h(x, \tau)$, given by Eqs. (26)-(28) at rescaled times $\tau/t = 0.35$ (top), 0.5 (middle) and 0.65 (bottom).

rected polymer in a random potential at high temperature with a large-deviation Monte Carlo sampling algorithm, we were able to observe the optimal paths of the KPZ interface which determine each two tails of the one-point height distribution $\mathcal{P}(H, t)$ at short times. Our algorithm allows one to probe the optimal paths

which are responsible for extremely unlikely events, with probability densities down to 10^{-500} . We clearly observed mirror-symmetry-broken “traveling-ramp” optimal interface height profiles for the higher tail, and mirror-symmetric paths for the lower tail, in good quantitative agreement with analytical predictions from the OFM. Alongside with Ref. [34], the present work illustrates the versatility, robustness and a great predictive power of the OFM in the description of large deviations of time-dependent non-equilibrium random fields.

Simulation-wise our work, alongside with Ref. [34], shows that, by using large-deviation approaches, one can not only reliably determine extremely small probabilities but also sample complete realizations from the extreme tails of corresponding distributions. This gives a valuable insight into the causes of extreme behavior of stochastic systems far from equilibrium. In the present case this is clear, because the OFM predicts an intimate connection between extremely small probabilities of observing very large $|H|$ and extremely rare interface configuration histories that are responsible for them. But the possibility to determine causal relations certainly also exists when no theoretical predictions are available, as was shown, *e.g.*, by large-deviation studies of stability conditions for energy grids [43, 44]. Furthermore, even if no clear causal relations emerge, large-deviation approaches allow for a much enlarged view into the correlations of systems.

ACKNOWLEDGMENTS

The simulations were performed in Oldenburg on the HPC cluster CARL which is funded by the DFG through its Major Research Instrumentation Programme (INST 184/157-1 FUGG) and the Ministry of Science and Culture (MWK) of the Lower Saxony State. The research of B.M. was supported by the Israel Science Foundation (grant No. 1499/20). The research of P.S. is supported by the project “High Field Initiative” (CZ.02.1.01/0.0/0.0/15.003/0000449) of the European Regional Development Fund.

[1] G. Schütz, in “*Phase Transitions and Critical Phenomena*”, edited by C.Domb and J. L. Lebowitz (Academic Press, London, 2001), Vol. 19.
[2] B. Derrida, J. Stat. Mech. (2007) P07023.
[3] P. I. Hurtado, C. P. Espigares, J. J. del Pozo, and P. L. Garrido, J. Stat. Phys. **154**, 214 (2014).
[4] L. Bertini, A. De Sole, D. Gabrielli, G. Jona-Lasinio, and C. Landim, Rev. Mod. Phys. **87**, 593 (2015).
[5] Y. Baek and Y. Kafri, J. Stat. Mech. (2015) P08026.
[6] M. Janas, A. Kamenev, and B. Meerson, Phys. Rev. E **94**, 032133 (2016).

[7] N. R. Smith, A. Kamenev, and B. Meerson, Phys. Rev. E **97**, 042130 (2018).
[8] M. Kardar, G. Parisi, and Y.-C. Zhang, Phys. Rev. Lett. **56**, 889 (1986).
[9] The height of the evolving KPZ interface has a systematic x -independent component $h_s(t)$. For a δ -correlated noise the derivative $dh_s(t)/dt$ is infinite. For a finite correlation length of the noise $dh_s(t)/dt$ approaches, at long times, a nonuniversal constant [11, 49, 50]. It is customary to get rid of this nuisance by defining $H = h(0, t) - h_s(t) - h(0, 0)$, and this is what we actually do here.

- [10] J. Quastel and H. Spohn, J. Stat. Phys. **160**, 965 (2015).
- [11] H. Spohn, in “*Stochastic Processes and Random Matrices*”, Lecture Notes of the Les Houches Summer School, Vol. 104, edited by G. Schehr, A. Altland, Y. V. Fyodorov, and L. F. Cugliandolo (Oxford University Press, Oxford, 2015), p. 177; arXiv:1601.00499.
- [12] K. A. Takeuchi, Physica A (Amsterdam) **504**, 77 (2018).
- [13] Formally, the short time regime corresponds to a strong inequality $t \ll t_{\text{NL}}$. Numerical simulations [33, 35] show, however, that the crossover from the short-time regime to the long-time regime actually occurs at $t/t_{\text{NL}} \simeq 64$.
- [14] Without loss of generality, we can pin the Brownian interface at the origin so that $h(0, 0) = 0$.
- [15] A. Krajenbrink and P. Le Doussal, Phys. Rev. E **96**, 020102(R) (2017).
- [16] T. Imamura and T. Sasamoto, Phys. Rev. Lett. **108**, 190603 (2012); J. Stat. Phys. **150**, 908 (2013).
- [17] A. Borodin, I. Corwin, P.L. Ferrari, and B. Vető, Math. Phys. Anal. and Geom. **18**, 1 (2015).
- [18] The one-point height distribution $\mathcal{P}(H, t)$ for the stationary KPZ interface belongs to a short list of exceptional objects for which *exact* representations are known. Using such a representation for the stationary interface [16, 17], Krajenbrink and Le Doussal [15] extracted the complete short-time large deviation function $S(H)$. In particular, they verified the predictions of Ref. [6] concerning the second-order DPT at $H = H_c$ and the two tail asymptotics (6) and (7). They also determined the value of H_c analytically.
- [19] I. V. Kolokolov and S. E. Korshunov, Phys. Rev. B **75**, 140201(R) (2007).
- [20] I. V. Kolokolov and S. E. Korshunov, Phys. Rev. B **78**, 024206 (2008).
- [21] I. V. Kolokolov and S. E. Korshunov, Phys. Rev. E **80**, 031107 (2009).
- [22] B. Meerson, E. Katzav, and A. Vilenkin, Phys. Rev. Lett. **116**, 070601 (2016).
- [23] A. Kamenev, B. Meerson, and P. V. Sasorov, Phys. Rev. E **94**, 032108 (2016).
- [24] B. Meerson and J. Schmidt, J. Stat. Mech. (2017) P103207.
- [25] N. R. Smith, B. Meerson, and P.V. Sasorov, J. Stat. Mech. (2018) 023202.
- [26] B. Meerson, P. V. Sasorov, and A. Vilenkin, J. Stat. Mech. (2018) 053201.
- [27] N. R. Smith and B. Meerson, Phys. Rev. E **97**, 052110 (2018).
- [28] B. Meerson and A. Vilenkin, Phys. Rev. E **98**, 032145 (2018).
- [29] T. Asida, E. Livne, and B. Meerson, Phys. Rev. E **99**, 042132 (2019).
- [30] N. R. Smith, B. Meerson, and A. Vilenkin, J. Stat. Mech. (2019) 053207.
- [31] Until very recently, analytical solutions of the OFM equations for the KPZ interface were only based on additional small parameters, such as a very large or very small $|H|$. In Ref. [51] the exact short-time large-deviation function for $\mathcal{P}(H, t)$ has been obtained for the droplet initial condition by masterfully exploiting exact integrability of the OFM equations noticed in Ref. [6].
- [32] A. K. Hartmann, *Big Practical Guide to Computer Simulations*, World Scientific, Singapore (2015).
- [33] A. K. Hartmann, P. Le Doussal, S. N. Majumdar, A. Rosso, and G. Schehr, Europhys. Lett. **121**, 67004 (2018).
- [34] A. K. Hartmann, B. Meerson, and P. Sasorov, Phys. Rev. Res. **1**, 032043(R) (2019).
- [35] A. K. Hartmann, A. Krajenbrink, and P. Le Doussal, Phys. Rev. E **101**, 012134 (2020).
- [36] P. Calabrese, P. Le Doussal, and A. Rosso, Europhys. Lett. **90**, 20002 (2010).
- [37] J. M. Hammersley and K. W. Morton, Math. Proc. Camb. Phil. Soc **52**, 449 (1956).
- [38] A. K. Hartmann, Phys. Rev. E **65**, 056102 (2002).
- [39] A. K. Hartmann, Eur. Phys. J. B **84**, 627-634 (2011).
- [40] A. K. Hartmann and M. Mézard, Phys. Rev. E **97**, 032128 (2018).
- [41] A. K. Hartmann, S. Majumdar, and A. Rosso, Phys. Rev. E **88**, 022119 (2013).
- [42] G. Claussen, A. K. Hartmann, and S. N. Majumdar, Phys. Rev. E **91**, 052104 (2015).
- [43] T. Dewenter and A.K. Hartmann, New J. Phys **17**, 015005 (2015).
- [44] Y. Feld and A. K. Hartmann, Chaos **29**, 113103 (2019).
- [45] S. Wolfsheimer, B. Burghardt and A. K. Hartmann, Algor. Mol. Biol. **2**, 2 (2007).
- [46] A. K. Hartmann, Phys. Rev. E **89**, 052103 (2014).
- [47] W. Staffeldt and A. K. Hartmann, Phys. Rev. E **100**, 062301 (2019).
- [48] M. E. J. Newman and G. T. Barkema, *Monte Carlo Methods in Statistical Physics* (Clarendon Press, Oxford, 1999).
- [49] T. Gueudré, P. Le Doussal, A. Rosso, A. Henry, and P. Calabrese, Phys. Rev. E **86**, 041151 (2012).
- [50] M. Hairer, Annals of Math. **178**, 559 (2013).
- [51] A. Krajenbrink and P. Le Doussal, arXiv:2103.17215.